



Strathprints Institutional Repository

Ginnis, A.I. and Kostas, K.V. and Politis, C.G. and Kaklis, P.D. and Belibassakis, K.A. and Gerostathis, Th.P. and Scott, M.A. and Hughes, T.J.R. (2014) Isogeometric boundary-element analysis for the wave-resistance problem using T-splines. Computer Methods in Applied Mechanics and Engineering, 279. pp. 425-439. ISSN 0045-7825 , <http://dx.doi.org/10.1016/j.cma.2014.07.001>

This version is available at <http://strathprints.strath.ac.uk/51258/>

Strathprints is designed to allow users to access the research output of the University of Strathclyde. Unless otherwise explicitly stated on the manuscript, Copyright © and Moral Rights for the papers on this site are retained by the individual authors and/or other copyright owners. Please check the manuscript for details of any other licences that may have been applied. You may not engage in further distribution of the material for any profitmaking activities or any commercial gain. You may freely distribute both the url (<http://strathprints.strath.ac.uk/>) and the content of this paper for research or private study, educational, or not-for-profit purposes without prior permission or charge.

Any correspondence concerning this service should be sent to Strathprints administrator: strathprints@strath.ac.uk

Isogeometric Boundary-Element Analysis for the Wave-Resistance Problem using T-splines

A.I. Ginnis^{a,*}, K.V. Kostas^b, C.G. Politis^b, P.D. Kaklis^{a,c}, K.A. Belibassakis^a,
Th.P. Gerostathis^b, M.A. Scott^d, T.J.R Hughes^e

^a*School of Naval Architecture & Marine Engineering, National Technical University of Athens*

^b*Department of Naval Architecture, Technological Educational Institute of Athens*

^c*Department of Naval Architecture, Ocean and Marine Engineering, University of Strathclyde*

^d*Department of Civil and Environmental Engineering, Brigham Young University*

^e*Institute for Computational Engineering and Sciences, The University of Texas at Austin*

Abstract

In this paper we couple collocated Boundary Element Methods (BEM) with unstructured analysis-suitable T-spline surfaces for solving a linear Boundary Integral Equation (BIE) arising in the context of a ship-hydrodynamic problem, namely the so-called Neumann-Kelvin problem, following the formulation by Brard (1972) [1] and Baar & Price (1988) [2]. The local-refinement capabilities of the adopted T-spline bases, which are used for representing both the geometry of the hull and approximating the solution of the associated BIE, in accordance with the Isogeometric concept proposed by Hughes et al. (2005) [3], lead to a solver that achieves the same error level for many fewer degrees of freedom as compared with the corresponding NURBS-based Isogeometric-BEM solver recently developed in Belibassakis et al. (2013) [4]. In this connection, this paper makes a step towards integrating modern CAD representations for ship-hulls with hydrodynamic solvers of improved accuracy and efficiency, which is a prerequisite for building efficient ship-hull optimizers.

1. Introduction

Wave-making resistance is a very important component, which may contribute up to 50% - or even more - to the total resistance of a ship, especially for relatively “full” hull forms and/or at high speeds. Experience has shown that the wave-making resistance component is quite sensitive to changes to hull-form shape and significant reduction can be achieved without affecting cargo capacity. During the last 50 years, the interest in numerical methods for calculating ship wave resistance has been constantly growing. Computations are performed using a variety of techniques, ranging from the simple Michell’s thin-ship theory [5] to extremely complex and costly methods such as the fully non-linear Reynolds Averaged Navier Stokes Equations (RANSE) [6, 7, 8]; see the reports by the International Towing Tank Conference ([9, 10, 11]) and the references cited therein.

*Corresponding author: ginnis@naval.ntua.gr

1
2
3
4
5
6
7
8 In all proposed methods a CAD model of the ship hull is required. However, analysis-suitable
9 models cannot be, in general, automatically derived from CAD models. Data exchange between
10 CAD and analysis methods requires many time-consuming, preparatory steps. For example, the
11 popular meshing approach is generally time consuming and provides only an approximation of
12 the exact CAD geometry. Furthermore, a recalculation of the generated mesh is required for
13 even slight changes in the exact geometry. Thus, the lack of geometric exactness along with the,
14 generally, cumbersome mesh regeneration render the requirements for rapid convergence and/or
15 high precision prohibitive. These deficiencies in the current engineering analysis approach also
16 preclude successful application of other procedures such as design optimization. In this case, the
17 CAD-geometry-to-mesh mapping needs to be automatic and tightly integrated with the analysis
18 solver and the optimizing environment. Enabling the automatic generation of geometrically exact
19 and analysis suitable models could pave the way towards overcoming the aforementioned barriers.
20 This aim can be achieved by appealing to IsoGeometric Analysis (IGA), introduced by Hughes
21 et al. [12, 3] and Cottrell et al. [13, 14], which provides a direct and tight link between CAD
22 and Computer Aided Engineering (CAE). This link is achieved by using the very same basis for
23 representing both the geometry and the physical quantities employed in the analysis.
24
25

26 A number of candidate geometry representations can be used in the context of IGA. The
27 geometrical representation, that is so far prevailing in CAD industry, is NURBS (Non-Uniform
28 Rational B-Splines) [15]. NURBS representations offer: 1) convenience in modeling free-form
29 parametric surfaces, 2) exact representation of all quadratic curves and surfaces that frequently
30 occur in Mechanical-Engineering Design and 3) availability of many efficient and numerically-stable
31 algorithms for their evaluation. NURBS also possess some mathematical properties that are useful
32 from the analysis point of view: a) refinability, such as the conventional h - (knot insertion) and
33 p - (degree elevation) refinement schemes, as well as a more flexible refinement pattern, the so-
34 called k -refinement, which is suitable for higher-order approximations, and b) high smoothness,
35 i.e., C^{p-1} -continuity for NURBS of degree $p \geq 2$, which prohibits derivative-jumps, thus, yielding
36 more accurate results.
37
38

39 Isogeometric Analysis has been so far mainly applied in the FEM context, [13, 3], where
40 the basic preprocessing step is to develop good quality two- and three-dimensional (trivariate)
41 representations of the computational domain. The latter is far from being a trivial problem and
42 although different methods have been developed, e.g., lofting, swept-volume parameterization,
43 Coons patches, etc., the literature is still lacking of a general and mature methodology. On the
44 other hand, this approach differs from that adopted in contemporary CAD systems, namely the
45 so-called Boundary representation (B-rep) of solids. In order to overcome these difficulties, a new
46 approach for exploiting Isogeometric analysis has been presented. It is based on the boundary
47 integral formulation of the problem considered, where the governing equations and the boundary
48
49
50
51
52
53
54
55
56
57
58
59
60
61
62
63
64
65

1
2
3
4
5
6
7
8 conditions of the problem are transformed into a boundary integral equation (weakly singular
9 or singular) on the boundary (or a portion of the boundary) using the Green’s function of the
10 problem to be treated [16, 17, 4, 18, 19, 20, 21]. This approach is widely used in free-surface
11 hydrodynamics, and especially in exterior potential-flow problems, due to the infinite extent of
12 the fluid domain.
13
14

15 In the above context, our previous work [4], has demonstrated the applicability and advantages
16 of the Isogeometric approach to free-surface problems and especially to a linearized version of the
17 wave-resistance problem, the so called “Neumann-Kelvin wave-resistance” problem, as initially
18 proposed by Brard (1972) [1]. In this version of the problem, the potential flow theory is adopted
19 and the non-linear effects stemming from the presence of the unknown free surface are neglected,
20 while the three-dimensional character of the problem is retained. For the numerical solution of
21 the resulting linear problem a Boundary-Element Method (BEM) was formulated, implemented
22 by means of a Kelvin-wave source distribution over the wetted part of the hull and its intersection
23 with the undisturbed free surface [2]. A multi-patch tensor product NURBS surface was used for
24 the representation of the wetted ship hull boundary and the very same NURBS basis was used
25 for the approximation of the unknown source density. The Isogeometric scheme was implemented
26 by collocating at the images of the Greville abscissae of the associated knot vectors and knot
27 insertion (h -refinement) is used as our refinement strategy. The enhanced accuracy and efficiency
28 of the proposed NURBS based IsoGeometric Analysis BEM (IGA-BEM) has been demonstrated
29 by comparing the numerical results obtained for a variety of geometrical configurations against
30 analytical solutions and/or experimental data (where available) as well as predictions provided by
31 low-order panel methods and higher-order BEMs. The tested configurations included a prolate
32 spheroid in an infinite domain, a three-axial ellipsoid in a semi-infinite domain, a submerged
33 prolate spheroid under the free surface and three free-surface piercing hulls, namely the standard
34 Wigley hull, a Series 60 and the so-called KRISO container ship hull [22].
35
36
37
38
39
40
41
42
43
44
45
46

47 However, the use of NURBS in Isogeometric Analysis exhibits some deficiencies:
48

- 49 1. Multi-patch representations suffer from gaps and overlaps at patch boundaries.
- 50
51 2. Due to their tensor-product nature a large number of NURBS control points is not unlikely
52 to be superfluous, in the sense that they contain no significant geometric information. As
53 a consequence, the resulting basis for approximating the physical quantities of interest, is
54 “overloaded” with redundant detail in areas where these quantities are expected to exhibit
55 low variation.
56
57 3. Refinement requires the insertion of entire rows/columns of control points, thus increasing
58 complexity and implementation effort.
59
60
61
62
63
64
65

- 1
 - 2
 - 3
 - 4
 - 5
 - 6
 - 7
 - 8
 - 9
 - 10
 - 11
 - 12
 - 13
 - 14
 - 15
 - 16
 - 17
 - 18
 - 19
 - 20
 - 21
 - 22
 - 23
 - 24
 - 25
 - 26
 - 27
 - 28
 - 29
 - 30
 - 31
 - 32
 - 33
 - 34
 - 35
 - 36
 - 37
 - 38
 - 39
 - 40
 - 41
 - 42
 - 43
 - 44
 - 45
 - 46
 - 47
 - 48
 - 49
 - 50
 - 51
 - 52
 - 53
 - 54
 - 55
 - 56
 - 57
 - 58
 - 59
 - 60
 - 61
 - 62
 - 63
 - 64
 - 65
4. The limitations of rectangular topology lead to multi-patch representations when complex objects, as e.g., ship hulls, are under consideration. This limitation has an additional side-effect as multi-patch configurations can only secure a C^0 basis continuity across patch boundaries, canceling, in this way, the intrinsic higher smoothness of a single NURBS patch.

T-splines [23, 24] constitute a recently developed generalization of NURBS technology that removes most of the above mentioned NURBS deficiencies. It is worth noticing that in the computer-aided ship-design literature one can already cite works arguing that NURBS do not offer the proper frame for ship design [25] and aspire to alternative representations, which include T-splines [26]. The main advantages of T-splines technology are:

1. T-splines permit representation of complex objects with a single T-spline patch.
2. A T-spline control grid is allowed to have partial rows of control points, terminating in T-junctions, which allows for local refinement.
3. T-junctions permit the significant reduction of superfluous control points.
4. It is possible to merge multiple NURBS patches into a single, gap-free T-spline.

Our aim in the present work is to make a first step towards exploiting the advantages of T-splines technology in Isogeometric analysis (TS-IGA) for ship hydrodynamic analysis. The higher smoothness of a single T-spline surface along with the ability for local refinement allow us to achieve enhanced convergence rates with considerably fewer degrees of freedom when compared to our prior NURBS approach. This will permit our T-spline based IGA-BEM solver to be embedded with significantly lower cost in any optimization process for designing ship hulls with minimum wave resistance.

The remaining part of this paper is structured in 4 sections. Section 2 presents the formulation of the problem while section 3 provides a brief overview of T-splines. We then proceed with the formulation of the problem in the Isogeometric T-spline BEM (TS-IGA-BEM) context and we conclude our work with two numerical examples demonstrating the achieved enhanced convergence: a prolate spheroid in infinite domain and a surface piercing ship hull.

2. Formulation of the problem

Let $Oxyz$ be a right-handed rectangular coordinate system with the z -axis directed vertically upwards; see Figure 1. We consider the flow of a uniform stream with velocity $\mathbf{U} = (-U, 0, 0)$ of an ideal fluid with a free surface incident upon a surface piercing or fully submerged body D .

It is convenient to decompose the velocity potential Φ in the form:

$$\Phi = -Ux + \varphi, \tag{1}$$

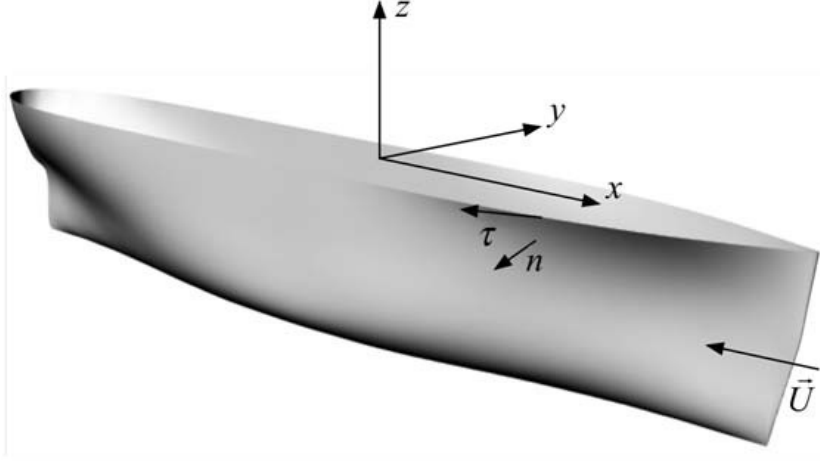


Figure 1: Geometric configuration of the Neumann-Kelvin problem for a surface piercing body.

where φ is the disturbance potential due to the presence of the submerged body. The disturbance potential must satisfy the Laplace equation (see, e.g., [2]):

$$\Delta\varphi = 0 \quad \text{in } D^+, \quad (2)$$

where D^+ denotes the unbounded fluid domain outside the body D limited above by the plane $z = 0$. The body boundary condition is

$$\frac{\partial\varphi}{\partial\mathbf{n}} = -\mathbf{U} \cdot \mathbf{n} \quad \text{on } S, \quad (3)$$

where $\mathbf{n} = (n_x, n_y, n_z)$ is the unit normal directed inwards with respect to the domain D^+ and $S = \partial D$ is the boundary of the body D . The free-surface conditions satisfied on the unknown free surface $z = \eta(x, y)$ are:

- (i) The kinematic condition, stating that on the free surface the flow velocity must be tangential:

$$(-U + \varphi_x)\eta_x + \varphi_y\eta_y - \varphi_z = 0. \quad (4)$$

- (ii) The dynamic condition, stating that the pressure on the free surface must be constant:

$$g\eta - U\varphi_x + \frac{1}{2}(\varphi_x^2 + \varphi_y^2 + \varphi_z^2) = 0, \quad (5)$$

with g denoting the gravitational acceleration. In the theory of infinitesimal waves the above conditions on the free surface are linearized by neglecting products and squares of “small” quantities (stemming from the fact that the disturbance velocities are considered to be of higher order with respect to U) and by applying the resulting equations on the undisturbed free surface $z = 0$

instead of the unknown free surface $z = \eta(x, y)$. Thus, equations (4) and (5) become, respectively,

$$U\eta_x + \varphi_z = 0, \quad (6)$$

$$g\eta - U\varphi_x = 0, \quad (7)$$

which can be combined to form the following linear free-surface condition:

$$\varphi_{xx} + k\varphi_z = 0 \quad \text{on} \quad z = 0. \quad (8)$$

Here $k = g/U^2$ is the characteristic wavenumber, controlling the wavelength of the transverse ship waves and is proportional to the inverse square of the corresponding Froude number $F = U/\sqrt{gL}$, with L denoting the maximum length of the body.

Finally, a radiation condition must be imposed in order to ensure existence and uniqueness of the disturbance potential. This condition expresses that waves radiated by the body are directed downwards and there are no upstream waves. Mathematically, this condition is expressed as follows:

$$\varphi = \begin{cases} O(1/|x|) \\ o(1) \end{cases} \quad \text{as} \quad |x| \rightarrow \infty, \quad \text{if} \quad \begin{cases} x < 0 & \text{(downstream),} \\ x > 0 & \text{(upstream).} \end{cases} \quad (9)$$

Following the approach initiated by Brard (1972) [1] and explored in [2] for the linearized Neumann-Kelvin wave-resistance problem, the disturbance potential φ may be represented as

$$\varphi(\mathbf{P}) = \int_S \mu(\mathbf{Q})G(\mathbf{P}, \mathbf{Q})dS(\mathbf{Q}) + \frac{1}{k} \int_\ell \mu(\mathbf{Q})G^*(\mathbf{P}, \mathbf{Q})n_x(\mathbf{Q})\tau_y(\mathbf{Q})d\ell(\mathbf{Q}), \quad P \in D^+, \quad (10)$$

where μ is the density of the single-layer distribution on the wetted body boundary S and ℓ is the waterline of S , which exists only in the case of a surface piercing body. In the above equation $G(\mathbf{P}, \mathbf{Q})$ denotes the associated Green's function of the Neumann-Kelvin problem defined as:

$$4\pi G(\mathbf{P}, \mathbf{Q}) = r^{-1} - (r')^{-1} + G^*(\mathbf{P}, \mathbf{Q}), \quad \mathbf{Q} \in S, \quad \mathbf{P} \in D^+ \cup S, \quad (11)$$

where $r = \|\mathbf{P} - \mathbf{Q}\|$, $r' = \|\mathbf{P} - \mathbf{Q}'\|$ with \mathbf{Q}' denoting the image of \mathbf{Q} with respect to the undisturbed free surface $z = 0$ and $G^*(\mathbf{P}, \mathbf{Q})$ stands for the regular part of the Neumann-Kelvin Green's function, consisting of exponential decaying and wavelike components; for more details see Baar and Price (1988) [2]. Furthermore, $\tau = (\tau_x, \tau_y, \tau_z)$ denotes the tangent vector along the waterline ℓ , directed as shown in Figure 1.

The use of (11) enables automatic satisfaction of the linearized condition on the undisturbed free surface (Figure 1) and the conditions at infinity. Using all the above, the Neumann-Kelvin problem is equivalently reformulated as a BIE on the body boundary S , characterized by a weakly

singular kernel,

$$\frac{\mu(\mathbf{P})}{2} - \int_S \mu(\mathbf{Q}) \frac{\partial G(\mathbf{P}, \mathbf{Q})}{\partial n(\mathbf{P})} dS(\mathbf{Q}) - \frac{1}{k} \int_\ell \mu(\mathbf{Q}) \frac{\partial G^*(\mathbf{P}, \mathbf{Q})}{\partial n(\mathbf{P})} n_x(\mathbf{Q}) \tau_y(\mathbf{Q}) d\ell(\mathbf{Q}) = \mathbf{U} \cdot \mathbf{n}(\mathbf{P}),$$

$$\mathbf{P}, \mathbf{Q} \in S. \quad (12)$$

From the solution of the above integral equation, various quantities, such as velocity, pressure distribution and ship wave pattern can be obtained. Specifically, total flow velocity and pressure are readily obtained by

$$\mathbf{w} = \mathbf{U} + \nabla\varphi, \quad (13)$$

$$p = p_\infty + \frac{\rho}{2}(U^2 - \|\mathbf{w}\|^2) - \rho gz, \quad (14)$$

where ρ is the fluid density and p_∞ is the ambient pressure. The deviation of pressure p from p_∞ is measured via the non-dimensional pressure coefficient

$$C_p = \frac{p - p_\infty}{\frac{\rho}{2}U^2} = 1 - \frac{\|\mathbf{w}\|^2 + 2gz}{U^2}. \quad (15)$$

Finally, the free-surface elevation is obtained by

$$\eta(x, y) = (U/g) \cdot \varphi_x(x, y; z = 0). \quad (16)$$

We conclude this section by noting that in the case of a fully submerged body the above formulation should be modified by dropping the waterline integral in Eqs. (10) and (12).

3. T-splines: A brief introduction

In this section, we present a brief overview of T-spline technology. For additional details the interested reader is referred to Sederberg et al. (2003a,b) [23, 27], Sederberg et al. (2004) [28], Bazilevs et al. (2010) [24], Scott et al. (2011) [29] and Scott et al. (2012) [30]. In what follows we focus on cubic T-spline surfaces due to their predominance in industry. We denote the spatial and parametric dimensions by d_s and d_p , respectively. We denote an element index by e and the number of non-zero basis functions over an element e by n .

3.1. The unstructured T-mesh

An important object of interest underlying T-spline technology is the T-mesh. For surfaces, a T-mesh is a polygonal mesh and we will refer to the constituent polygons as elements or, equivalently, faces. Each element is a quadrilateral whose edges are permitted to contain T-junctions – vertices that are analogous to hanging nodes in finite elements. A control point, $\mathbf{P}_A \in \mathbb{R}^{d_s}$, $d_s = 2, 3$ and a control weight, $w_A \in \mathbb{R}$, where the index A denotes a global control point number, is assigned to every vertex in the T-mesh. The valence of a vertex is the number of

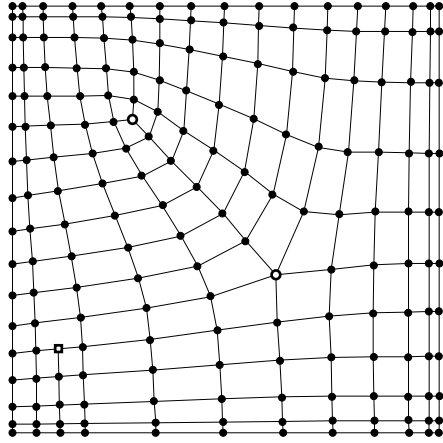


Figure 2: An unstructured T-mesh. Extraordinary points are denoted by hollow circles and T-junctions are denoted by hollow squares.

edges that touch the vertex. An extraordinary point is an interior vertex that is not a T-junction and whose valence does not equal four.

Figure 2 shows an unstructured T-mesh. Notice the valence three and valence five at extraordinary points denoted by hollow circles. The single T-junction is denoted by a hollow square.

To define a basis, a valid knot interval configuration must be assigned to the T-mesh. A knot interval is a non-negative real number assigned to an edge. A valid knot interval configuration requires that the knot intervals on opposite sides of every element sum to the same value. In this paper, we require that the knot intervals for spoke edges of an individual extraordinary point either be all non-zero or all zero.

3.2. Bézier extraction

In this paper, we develop T-splines from the finite element point-of-view, utilizing Bézier extraction [31, 29]. The idea is to extract the linear operator which maps the Bernstein polynomial basis on Bézier elements to the global T-spline basis. The linear transformation is defined by a matrix referred to as the extraction operator and denoted by \mathbf{C}^e . The transpose of the extraction operator maps the control points of the global T-spline to the control points of the Bernstein polynomials. Figure 3 illustrates the idea for a B-spline curve. This provides a finite element representation of T-splines, and facilitates the incorporation of T-splines into existing finite element programs. Only the shape function subroutine needs to be modified. All other aspects of the finite element program remain the same. Additionally, Bézier extraction is automatic and can be applied to any T-spline regardless of topological complexity or polynomial degree. In particular, it represents an elegant treatment of T-junctions, referred to as hanging nodes in finite element analysis.

1
2
3
4
5
6
7
8
9
10
11
12
13
14
15
16
17
18
19
20
21
22
23
24
25
26
27
28
29
30
31
32
33
34
35
36
37
38
39
40
41
42
43
44
45
46
47
48
49
50
51
52
53
54
55
56
57
58
59
60
61
62
63
64
65

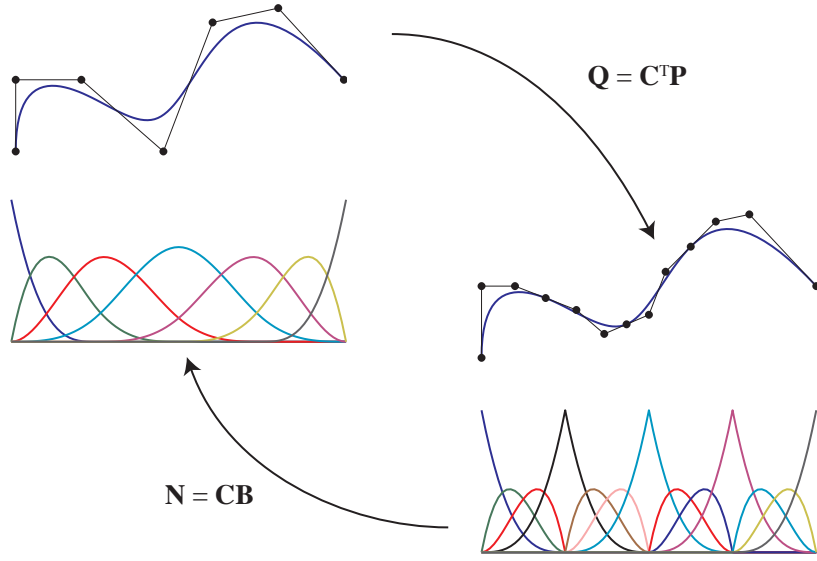


Figure 3: Schematic representation of Bézier extraction for a B-spline curve. B-spline basis functions and control points are denoted by \mathbf{N} and \mathbf{P} , respectively. Bernstein polynomials and control points are denoted by \mathbf{B} and \mathbf{Q} , respectively. The curve $T(\xi) = \mathbf{P}^T \mathbf{N}(\xi) = \mathbf{Q}^T \mathbf{B}(\xi)$.

3.3. The T-spline basis

A T-spline basis function, N_A , is defined for every vertex, A , in the T-mesh. Each N_A is a bivariate piecewise polynomial function. If A is not adjacent to an extraordinary point, N_A is comprised of a 4×4 grid of polynomials. Otherwise, the polynomials comprising N_A do not form a 4×4 grid but rather an unstructured grid of polynomials. In either case, the polynomials can be represented in Bézier form. Because of this, Bézier extraction can be applied to an entire T-spline to generate a finite set of Bézier elements such that

$$\mathbf{N}^e(\tilde{\xi}) = \mathbf{C}^e \mathbf{B}(\tilde{\xi}), \quad (17)$$

where $\tilde{\xi} \in \tilde{\Omega}$ is a coordinate in a standard Bézier parent element domain, $\mathbf{N}^e(\tilde{\xi}) = \{N_a^e(\tilde{\xi})\}_{a=1}^n$ is a vector of T-spline basis functions which are non-zero over Bézier element e , $\mathbf{B}(\tilde{\xi}) = \{B_i(\tilde{\xi})\}_{i=1}^m$ is a vector of tensor product Bernstein polynomial basis functions defining Bézier element e and $\mathbf{C}^e \in \mathbb{R}^{n \times m}$ is the element extraction operator.

3.4. The T-spline discretization

We can define the element geometric map, $\mathbf{X}^e : \tilde{\Omega} \rightarrow \Omega^e$, from the parent element domain onto the physical domain in the reference configuration as

$$\mathbf{X}^e(\tilde{\xi}) = \frac{1}{(\mathbf{w}^e)^T \mathbf{N}^e(\tilde{\xi})} (\mathbf{P}^e)^T \mathbf{W}^e \mathbf{N}^e(\tilde{\xi}) \quad (18)$$

$$= (\mathbf{P}^e)^T \mathbf{R}^e(\tilde{\xi}) \quad (19)$$

where $\mathbf{R}^e(\tilde{\boldsymbol{\xi}}) = \{R_a^e(\tilde{\boldsymbol{\xi}})\}_{a=1}^n$ is a vector of rational T-spline basis functions, the element weight vector $\mathbf{w}^e = \{w_a^e\}_{a=1}^n$, the diagonal weight matrix $\mathbf{W}^e = \text{diag}(\mathbf{w}^e)$, and \mathbf{P}^e is a matrix of dimension $n \times d_s$ that contains element control points,

$$\mathbf{P}^e = \begin{bmatrix} P_1^{e,1} & P_1^{e,2} & \dots & P_1^{e,d_s} \\ P_2^{e,1} & P_2^{e,2} & \dots & P_2^{e,d_s} \\ \vdots & \vdots & & \vdots \\ P_n^{e,1} & P_n^{e,2} & \dots & P_n^{e,d_s} \end{bmatrix}. \quad (20)$$

Using (18) and (19) we have that

$$\mathbf{R}^e(\tilde{\boldsymbol{\xi}}) = \frac{1}{(\mathbf{w}^e)^T \mathbf{N}^e(\tilde{\boldsymbol{\xi}})} \mathbf{W}^e \mathbf{N}^e(\tilde{\boldsymbol{\xi}}), \quad (21)$$

and using (17)

$$\mathbf{R}^e(\tilde{\boldsymbol{\xi}}) = \frac{1}{(\mathbf{w}^e)^T \mathbf{C}^e \mathbf{B}(\tilde{\boldsymbol{\xi}})} \mathbf{W}^e \mathbf{C}^e \mathbf{B}(\tilde{\boldsymbol{\xi}}). \quad (22)$$

Note that all quantities in (22) are written in terms of the Bernstein basis defined over the parent element domain, $\tilde{\Omega}$.

4. T-spline based Isogeometric BEM

The Isogeometric Analysis philosophy attempts to define the approximate field quantities (dependent variables) of the boundary-value problem in question from the basis that is being used for representing the geometry of the body boundary. In the case of the boundary integral equation (12), the dependent variable is the source-sink density μ , distributed over the body boundary S . The latter is accurately and efficiently represented as a T-spline surface, as below:

$$S = \bigcup_1^{n_e} S_e, \quad S_e(\tilde{\boldsymbol{\xi}}) = \sum_{i=1}^{n_{cp}} \mathbf{d}_i R_i^e(\tilde{\boldsymbol{\xi}}), \quad \tilde{\boldsymbol{\xi}} \in \tilde{\Omega}_e, \quad (23)$$

where n_{cp} is the number of control points, or T-mesh vertices, \mathbf{d}_i in the T-mesh, R_i^e is the restriction of the rational T-spline basis function R_i at $\tilde{\Omega}_e$, and n_e is the number of elements. In conformity with the IGA concept, the unknown source-sink surface distribution μ is approximated by the very same T-splines basis used for the body-boundary representation (23), that is:

$$\mu(\mathbf{P}) = \sum_{i=1}^{n_{cp}} \mu_i \tilde{R}_i(\mathbf{P}), \quad \mathbf{P} \in S, \quad (24)$$

where $\tilde{R}_i(\mathbf{P}) \equiv R_i^e(\tilde{\boldsymbol{\xi}}(\mathbf{P}))$, $\mathbf{P} \in S_e$. Inserting Eq. (24) into the BIE (12) we get:

$$\frac{1}{2} \sum_{i=1}^{n_{cp}} \mu_i \tilde{R}_i(\mathbf{P}) - \sum_{i=1}^{n_{cp}} \mu_i \mathbf{n}(\mathbf{P}) \cdot \mathbf{u}_i(\mathbf{P}) = \mathbf{U} \cdot \mathbf{n}(\mathbf{P}), \quad \mathbf{P} \in S, \quad (25)$$

where

$$\begin{aligned} \mathbf{u}_i(\mathbf{P}) = & \int_S \tilde{R}_i(\mathbf{Q}) \nabla_P G(\mathbf{P}, \mathbf{Q}) dS(\mathbf{Q}) + \\ & + k^{-1} \int_\ell \tilde{R}_i(\mathbf{Q}) \nabla_P G^*(\mathbf{P}, \mathbf{Q}) n_x(\mathbf{Q}) \tau_y(\mathbf{Q}) d\ell(\mathbf{Q}) \end{aligned} \quad (26)$$

are the so-called induced velocity factors.

We now collocate Eq. (25) by specifying n_{cp} collocation points $\mathbf{P}_j, j = 1, \dots, n_{cp}$, on S . For smooth ship hulls, these points correspond to the 1-ring collocation points defined for both the non-extraordinary and extraordinary vertices of the T-mesh. In this way, we obtain the following linear system of equations with respect to the unknown coefficients μ_i :

$$\sum_{i=1}^{n_{cp}} \mu_i \left[\tilde{R}_i(\mathbf{P}_j) - 2\mathbf{n}(\mathbf{P}_j) \cdot \mathbf{u}_i(\mathbf{P}_j) \right] = 2\mathbf{U} \cdot \mathbf{n}(\mathbf{P}_j), \quad j = 1, \dots, n_{cp}. \quad (27)$$

In the above equation, the integrals involved in the calculation of the induced velocity factors (Eq.26) are localized to element integrals over Bézier elements using the Bézier extraction framework described in §3.2. Moreover, we need to make sure that collocation point \mathbf{P}_j lies inside of such an element (and not on an edge) in order for the Cauchy Principal Value (CPV) integrals in Eq. 26) to exist. If this is not the case we appropriately shift automatically the corresponding collocation point so that the evaluation of the CPV integrals can be carried out.

5. Numerical Results and Discussion

In order to test the efficiency and accuracy of the T-spline BEM methodology developed in the previous sections, we shall now present and discuss its performance in tests involving an ellipsoid (§5.1) and a ship hull (§5.2). Efficiency will be investigated by comparing locally-refined T-splines with non-locally refined NURBS. The error will be compared with either analytically available solutions or reference solutions provided by the NURBS solver after a dense global refinement.

5.1. A prolate spheroid in an infinite domain

In this example, we consider a prolate spheroid with axes $a, b=c$, and ratio $a : b = 5 : 1$, moving at constant speed $\mathbf{U} = (-U, 0, 0)$ in an infinite homogeneous fluid. In this case, an analytical expression of the velocity \mathbf{w} on the surface of the ellipsoid is available, namely:

$$\mathbf{w}(\mathbf{P}) = \frac{2}{2 - a_0} (\mathbf{U} - U n_x(\mathbf{P}) \mathbf{n}(\mathbf{P})), \quad (28)$$

$$a_0 = \frac{1 - \epsilon^2}{\epsilon^3} \left(-2\epsilon + \ln \left(\frac{1 + \epsilon}{1 - \epsilon} \right) \right), \quad \epsilon = \sqrt{1 - (b/a)^2}; \quad (29)$$

(see e.g. [32, 33]). In our study the L^2 -error associated with the velocity field on the body surface is defined as follows:

$$\|\mathbf{w} - \mathbf{w}^r\|_{L^2} = \left(\int_S \|\mathbf{w}(\mathbf{P}) - \mathbf{w}^r(\mathbf{P})\|^2 dS(\mathbf{P}) \right)^{\frac{1}{2}} \quad (30)$$

where \mathbf{w}^r denotes the IGA-BEM approximation of \mathbf{w} corresponding to the refinement level r . Figure 4 depicts the T-mesh of the spheroid along with the corresponding pointwise error $\|\mathbf{w}(\mathbf{P}) - \mathbf{w}^r(\mathbf{P})\|$ of the velocity for five refinement steps. Each refinement level r is obtained by locally refining the T-mesh at level $r-1$ in areas where the error is high. This refinement process manages to reduce the L^∞ -error from 10^{-1} to 10^{-3} . The corresponding NURBS based process, where each T-mesh is replaced by its unique NURBS refinement, is given in Figure 5.

Figure 6 illustrates that, for a given level of L^2 -error, the T-spline based local refinement process requires considerably fewer degrees of freedom compared to the corresponding NURBS-based global refinement process (e.g., for an error of 5.5×10^{-4} the required degrees of freedom are approximately 600 for the T-spline vs. 1600 for the corresponding NURBS representation, i.e., a reduction of 62.5%).

1
2
3
4
5
6
7
8
9
10
11
12
13
14
15
16
17
18
19
20
21
22
23
24
25
26
27
28
29
30
31
32
33
34
35
36
37
38
39
40
41
42
43
44
45
46
47
48
49
50
51
52
53
54
55
56
57
58
59
60
61
62
63
64
65

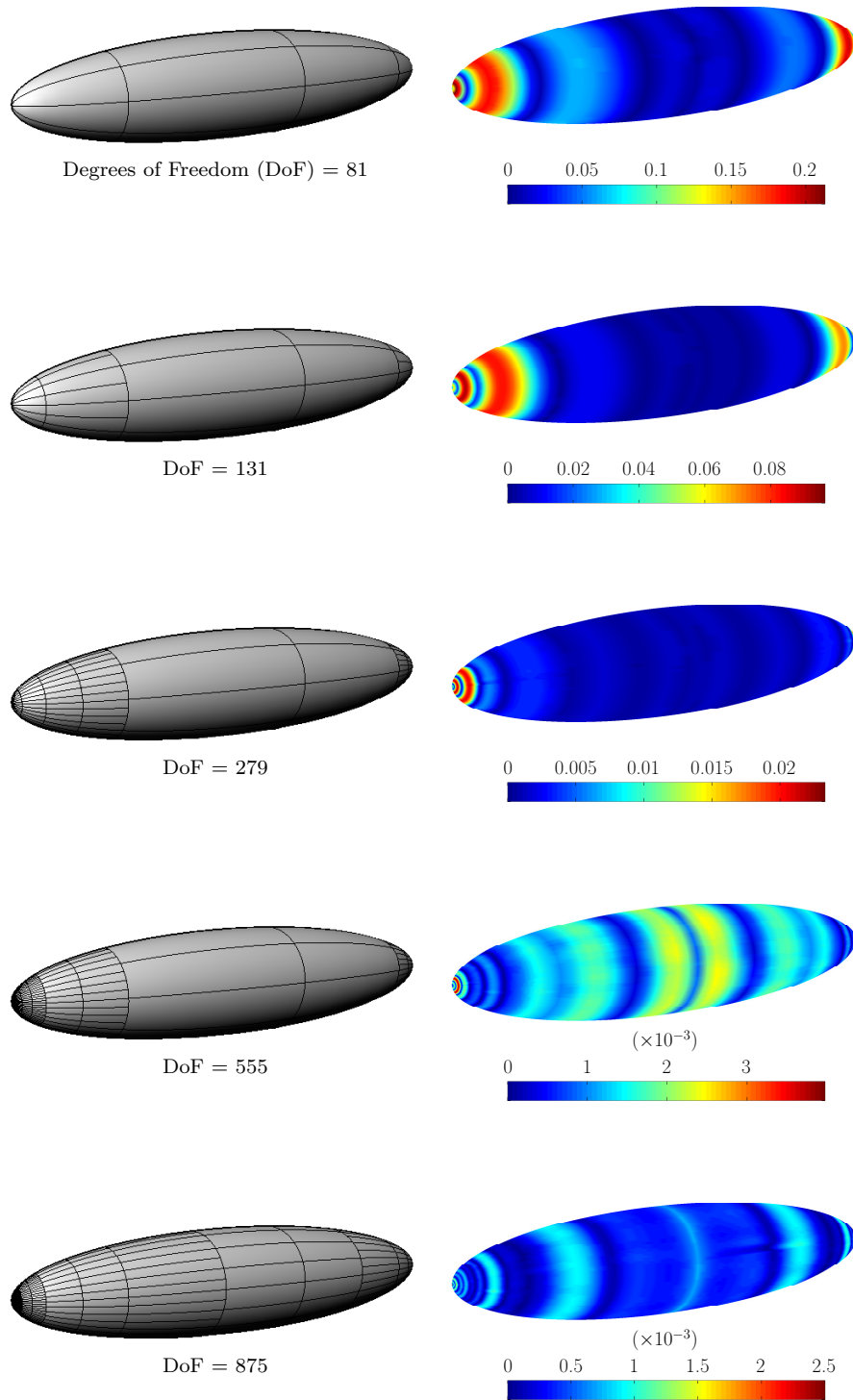


Figure 4: T-spline refinement steps (left column) along with the corresponding velocity error distribution (right column).

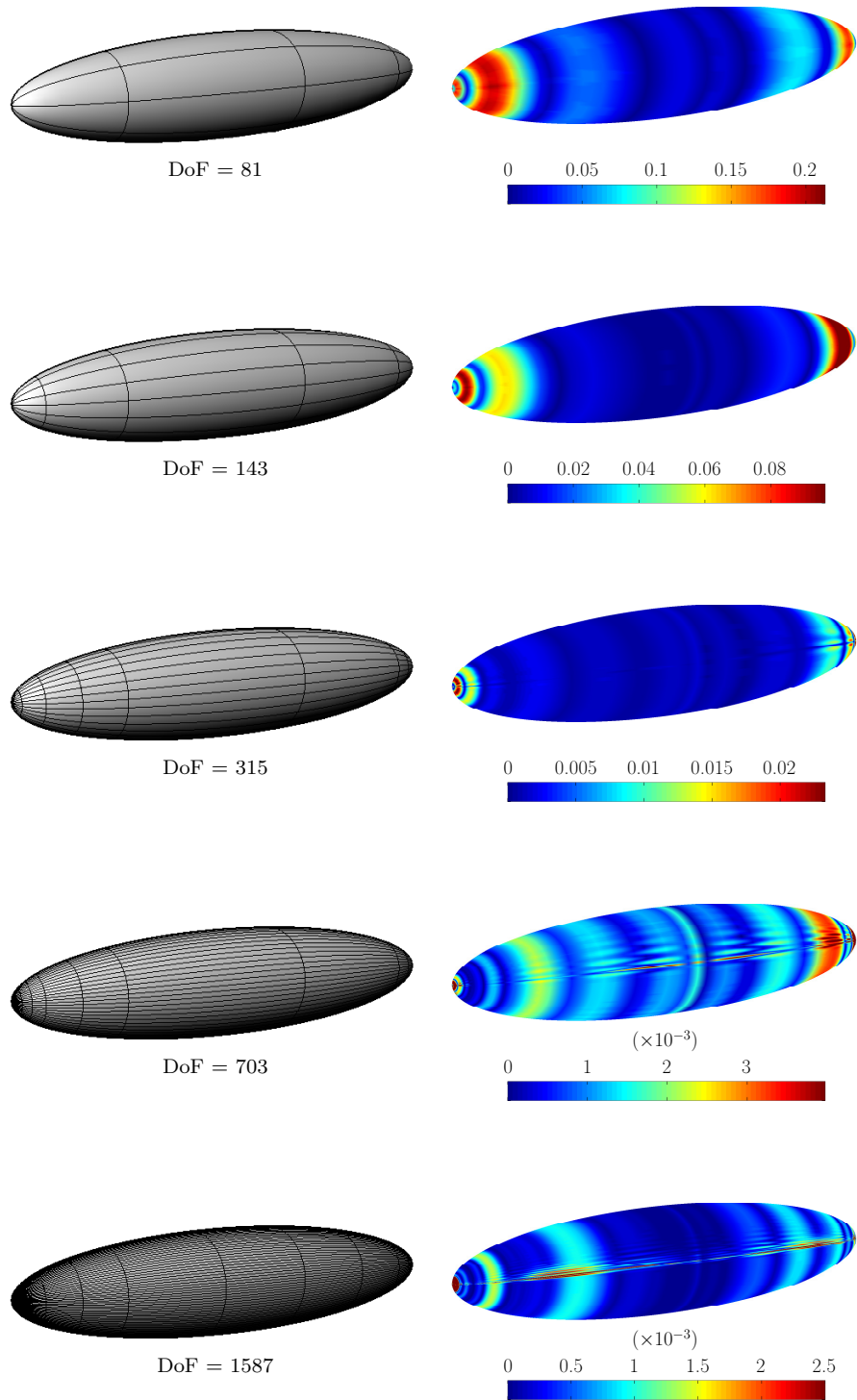


Figure 5: NURBS refinement steps (left column) along with the corresponding velocity error distribution (right column).

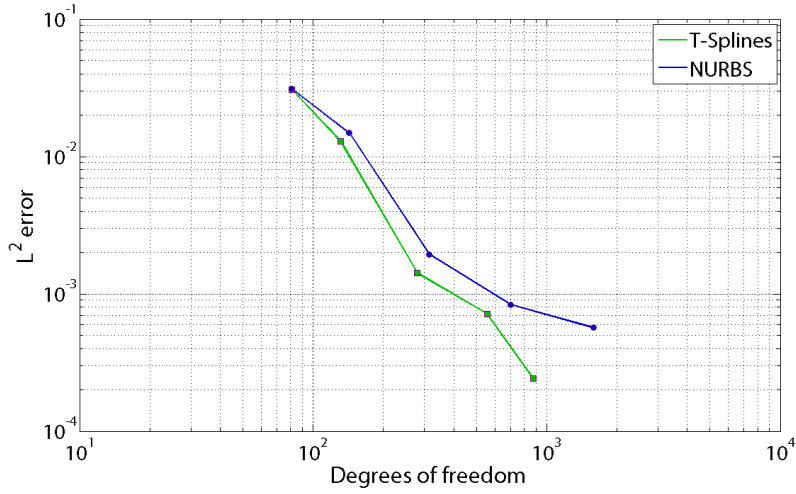


Figure 6: L^2 velocity error versus degrees of freedom corresponding to the refinement processes depicted in Figures 4 and 5. The T-spline meshes are locally refined based on comparison with the analytic solution. The NURBS results (blue curve) correspond to the unique NURBS refinement of each of the T-spline meshes.

5.2. Experimenting with a ship hull

In this example we consider a surface piercing ship moving with constant speed $\mathbf{U} = (U, 0, 0)$. The T-spline surface model of the ship hull has been constructed within the Rhinoceros modeling system¹ and more specifically by using its T-spline plugin². The resulting T-spline surface, see Figure 7(a), is locally of polynomial degree three in both directions and has 79 control points. Since all interior control points are either T-junctions or have a valence of four, no extraordinary control points exist in the T-mesh thus allowing a unique conversion of the T-spline representation into a single NURBS patch which comprises 132 control points; see Figure 7(b).

In order to drive a local refinement process and check the corresponding convergence rate of the solution, we have constructed a “reference solution” of the problem by inserting uniformly nine knots in every knot interval of the original NURBS representation and computing the IGA-BEM approximation of μ for the resulting NURBS surface. The obtained mesh along with the corresponding reference solution are depicted in Figure 8.

The L^2 -error associated with the distribution of the solution field μ on the body surface is defined as follows:

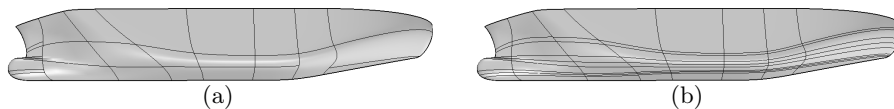
$$\|\mu_{ref} - \mu^r\|_{L^2} = \left(\int_S |\mu_{ref}(\mathbf{P}) - \mu^r(\mathbf{P})|^2 dS(\mathbf{P}) \right)^{\frac{1}{2}} \quad (31)$$

¹<http://www.rhino3d.com>

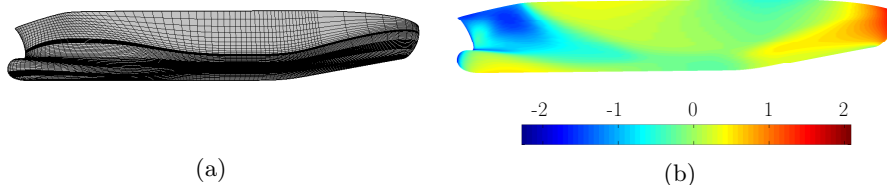
²<http://www.tsplines.com>

1
2
3
4
5
6
7
8 where μ_{ref} denotes the reference solution while μ^r denotes the IGA-BEM approximation of μ
9 corresponding to the refinement level r . The L^2 -error associated with the distribution of the
10 pressure coefficient C_p is analogously defined. Figure 9 depicts the T-mesh of the ship hull along
11 with the corresponding pointwise error $|\mu_{ref}(\mathbf{P}) - \mu^r(\mathbf{P})|$ of μ for the original mesh and three
12 refinement steps. Each refinement level r is obtained by locally refining the T-mesh at level $r - 1$
13 in areas where the error is high. In the first two steps the refinement is confined in the bow and
14 stern areas while the third one involves the middle part as well. The corresponding NURBS based
15 process, where each T-mesh is replaced by its unique NURBS refinement, is given in Figure 10.
16
17
18
19

20 In Figure 11a the L^2 -error for μ versus the degrees of freedom is presented for the T-spline
21 based local refinement process (blue curve), the corresponding NURBS refinement (red curve)
22 and the refinement process resulting from inserting uniformly r knots in each parametric interval
23 of the original NURBS representation (green curve). As it can be seen from this figure, for a
24 given error level, the T-spline based refinement requires considerably fewer degrees of freedom
25 as compared to the other two refinement processes. The worst performance occurs, as expected,
26 when using uniform refinement. Analogous remarks can be also made for the L^2 -error for C_p ,
27 which is presented in Figure 11(b).
28
29
30
31
32
33
34
35



40 Figure 7: T-spline (a) and NURBS (b) surface model of the ship hull.



50 Figure 8: Uniformly refined NURBS mesh(a) and corresponding reference solution (b).
51
52
53
54
55
56
57
58
59
60
61
62
63
64
65

1
2
3
4
5
6
7
8
9
10
11
12
13
14
15
16
17
18
19
20
21
22
23
24
25
26
27
28
29
30
31
32
33
34
35
36
37
38
39
40
41
42
43
44
45
46
47
48
49
50
51
52
53
54
55
56
57
58
59
60
61
62
63
64
65

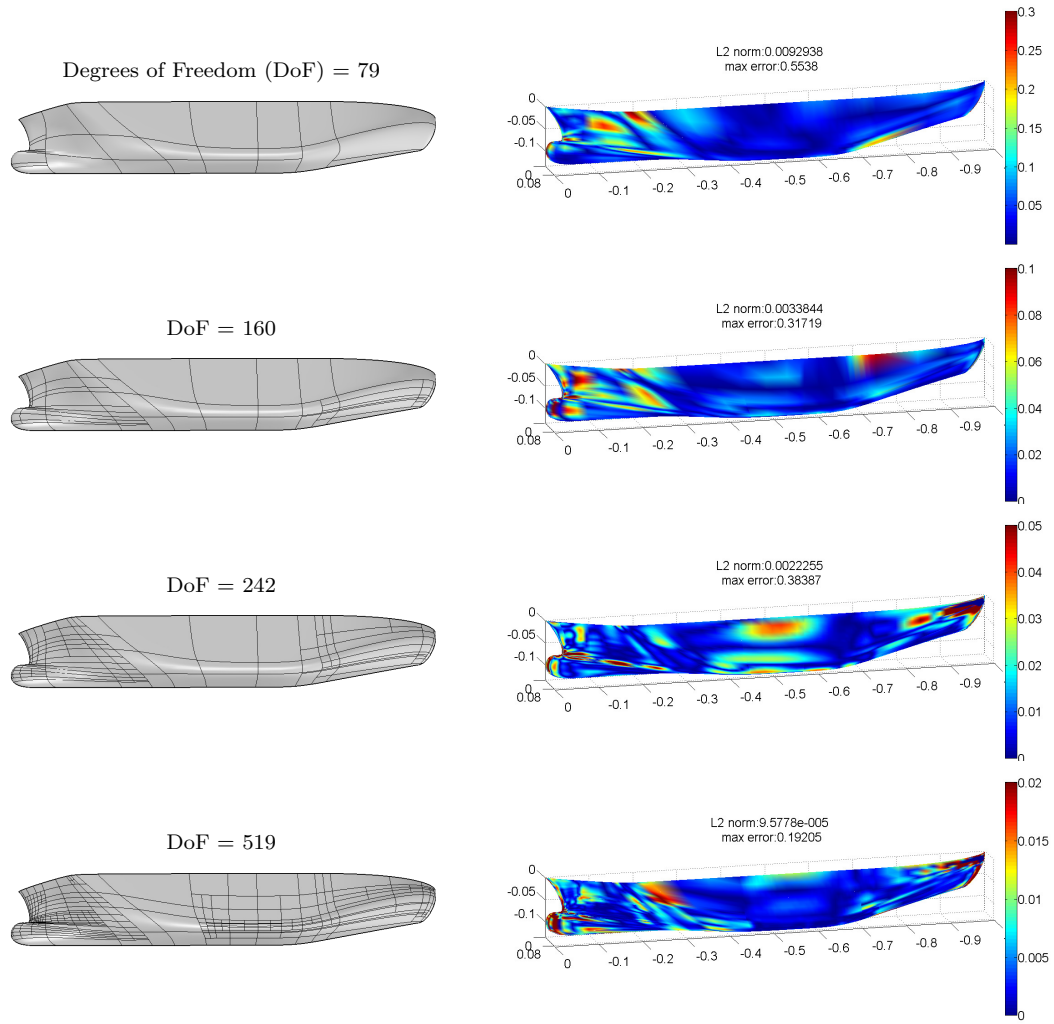


Figure 9: T-spline refinement steps (left column) along with the corresponding error distribution of the solution μ (right column).

1
2
3
4
5
6
7
8
9
10
11
12
13
14
15
16
17
18
19
20
21
22
23
24
25
26
27
28
29
30
31
32
33
34
35
36
37
38
39
40
41
42
43
44
45
46
47
48
49
50
51
52
53
54
55
56
57
58
59
60
61
62
63
64
65

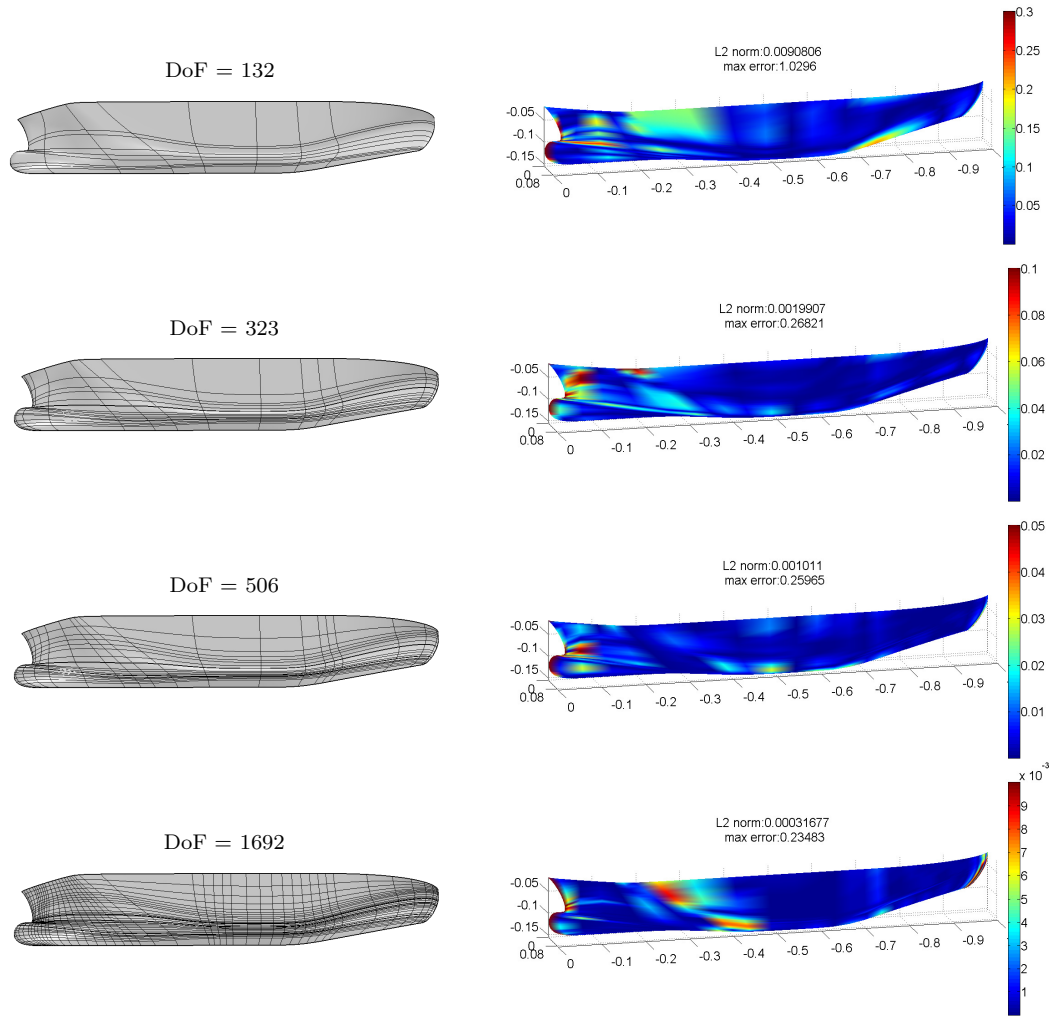
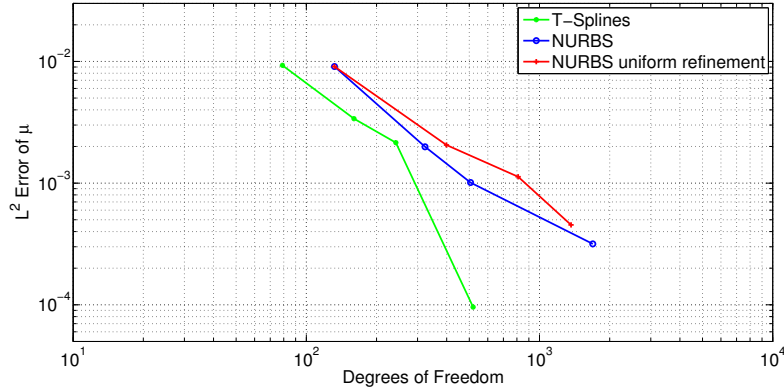
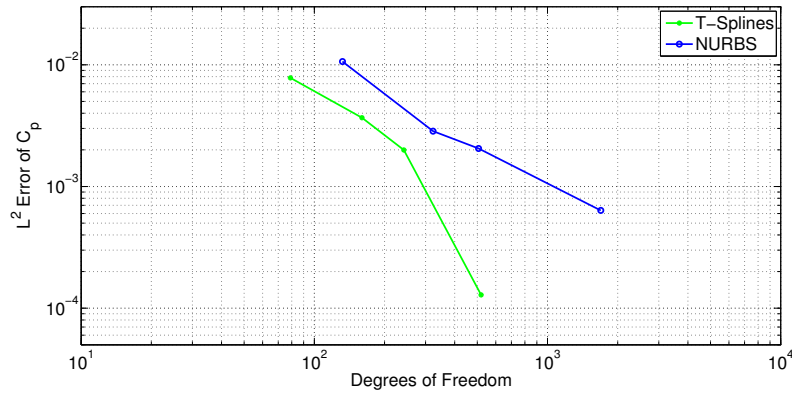


Figure 10: NURBS refinement steps (left column) along with the corresponding error distribution of the solution μ (right column).



(a)



(b)

Figure 11: L^2 -error of the density μ (a) and pressure coefficient C_p (b) versus the degrees of freedom corresponding to the refinement processes depicted in Figs. 9 and 10. The T-spline meshes are locally refined based on comparison with the reference solution. The NURBS results (blue curve) correspond to the unique NURBS refinement of each of the T-spline meshes. The NURBS uniform refinement (red curve in (a)) extends the coarsest T-spline to its unique NURBS refinement and then uniformly refines it.

6. Conclusions

In this work, we have demonstrated the advantages of T-splines technology in the context of the ship wave resistance calculation. The higher smoothness of the bases for a single T-spline surface along with the ability for local refinement allowed us to achieve enhanced convergence rates with considerably fewer degrees of freedom when compared to our prior NURBS approach. For the prolate spheroid example, the T-spline based local refinement process requires considerably fewer degrees of freedom compared to the corresponding NURBS-based global refinement process (e.g., for an error of 5.5×10^{-4} the required degrees of freedom are approximately 600 for T-spline vs. 1600 for the corresponding NURBS representation, i.e., a reduction of 62.5%; see Figure 6). The exact same picture is drawn from our second example, i.e., the ship hull.

1
2
3
4
5
6
7
8 This significant enhancement permits our T-spline based IGA-BEM solver to be embedded
9 with significantly lower cost in any optimization process for designing ship hulls with minimum
10 wave resistance; see, e.g. [34]. Future work will focus on this direction as well as on the extension
11 of the methodology to treat effects of nonlinearities in the wave resistance problem.
12
13

14 **References**

- 15
16
17 [1] R. Brard, The representation of a given ship form by singularity distributions when the
18 boundary condition on the free surface is linearized, *Ship Research* 16 (1972) 79–82.
19
20 [2] J. J. M. Baar, W. G. Price, Developments in the Calculation of the Wavemaking Resis-
21 tance of Ships, *Proc. Royal Society of London. Series A, Mathematical and Physical Sciences*
22 462 (1850) (1988) 115–147.
23
24 [3] T. Hughes, J. Cottrell, B. Y., Isogeometric analysis: CAD, finite elements, NURBS, exact
25 geometry and mesh refinement, *Computer Methods in Applied Mechanics and Engineering*
26 194 (2005) 4135–4195.
27
28 [4] K. A. Belibassakis, T. P. Gerosthathis, K. V. Kostas, C. G. Politis, P. D. Kaklis, A.-A.
29 Ginnis, C. Feurer, A BEM-Isogeometric method for the ship wave-resistance problem, *Ocean*
30 *Engineering* 60 (2013) 53–67.
31
32 [5] J. Michell, The wave resistance of a ship, *Philosophical Magazine* 45 (272).
33
34 [6] P. M. Carrica, R. V. Wilson, F. Stern, An Unsteady Single-Phase Level Set Method for
35 Viscous Free Surface Flows, *International Journal for Numerical Methods in Fluids* 53 (2)
36 (2007) 229–256.
37
38 [7] L. Larsson, F. Stern, V. Bertram, Benchmarking of Computational Fluid Dynamics for Ship
39 Flows: The Gothenburg 2000 Workshop, *Ship Research* 47 (1) (2003) 63–81.
40
41 [8] G. Tzabiras, Resistance and self-propulsion calculations for a series 60, cb060 hull at model
42 and full scale, *Ship Technology Research* 51 (2004) 21–34.
43
44 [9] I. R. Committee, Report of the Resistance Committee, in: *Proceedings of the 24th Interna-*
45 *tional Towing Tank Conference, 2005.*
46
47 [10] I. R. Committee, Report of the Resistance Committee, in: *Proceedings of the 25th Interna-*
48 *tional Towing Tank Conference, 2008.*
49
50 [11] I. R. Committee, Report of the Resistance Committee, in: *Proceedings of the 26th Interna-*
51 *tional Towing Tank Conference, 2011.*
52
53
54
55
56
57
58
59
60
61
62
63
64
65

- 1
2
3
4
5
6
7
8 [12] T. J. R. Hughes, Isogeometric analysis: Progress and Challenges, in: International Conference
9 on Mathematical Methods for Curves & Surfaces (MMCS08), Oslo, Norway, 2008.
10
11 [13] J. A. Cottrell, T. J. R. Hughes, Y. Bazilevs, Isogeometric Analysis: Toward Integration of
12 CAD and FEA, Wiley, 2009.
13
14 [14] J. A. Cottrell, T. J. R. Hughes, A. Reali, Studies of refinement and continuity in isogeometric
15 structural analysis, Computer Methods in Applied Mechanics and Engineering 196 (2007)
16 4160–4183.
17
18 [15] L. Piegl, W. Tiller, The Nurbs Book, 2nd Edition, Springer Verlag, 1997.
19
20 [16] C. Politis, A. Ginnis, P. Kaklis, K. Belibassakis, C. Feurer, An isogeometric BEM for exterior
21 potential-flow problems in the plane, in: 2009 SIAM/ACM Joint Conference on Geometric
22 and Physical Modeling, 2009.
23
24 [17] K. Belibassakis, T. Gerostathis, K. V. Kostas, C. Politis, P. D. Kaklis, A. I. Ginnis, C. Feurer,
25 A BEM-isogeometric method with application to the wavemaking resistance problem of ships
26 at constant speed, in: 30th International Conference on Offshore Mechanics and Arctic En-
27 gineering, 2011.
28
29 [18] R. Simpson, S. Bordas, J. Trevelyan, T. Rabczuk, A two-dimensional isogeometric boundary
30 element method for elastostatic analysis, Computer Methods in Applied Mechanics and En-
31 gineering 209-212 (0) (2012) 87 – 100. doi:<http://dx.doi.org/10.1016/j.cma.2011.08.008>.
32 URL <http://www.sciencedirect.com/science/article/pii/S0045782511002635>
33
34 [19] K. Li, X. Qian, Isogeometric analysis and shape optimization via boundary integral., CAD
35 43 (11) (2011) 1427–1437.
36
37 [20] M. A. Scott, R. N. Simpson, J. A. Evans, S. Lipton, S. P. A. Bordas, T. J. R.
38 Hughes, T. Sederberg, Isogeometric boundary element analysis using unstructured t-splines,
39 Computer Methods in Applied Mechanics and Engineering 254 (0) (2013) 197 – 221.
40 doi:<http://dx.doi.org/10.1016/j.cma.2012.11.001>.
41 URL <http://www.sciencedirect.com/science/article/pii/S0045782512003386>
42
43 [21] R. N. Simpson, M. A. Scott, M. Taus, D. C. Thomas, H. Lian, Acoustic isogeometric boundary
44 element analysis, Computer Methods in Applied Mechanics and Engineering 269 (2014) 265–
45 290.
46
47 [22] KRISO, Kriso container ship (kcs),
48 www.nmri.go.jp/institutes/fluid_performance_evaluation/cfd_rd/cfdws05/Detail/KCS/kcs_l&r.htm(1997).
49
50 [23] T. W. Sederberg, J. Zheng, A. Bakenov, A. Nasri, T-splines and TNURCCs, ACM Transac-
51 tions on Graphics 22 (2003) 477–484.
52
53
54
55
56
57
58
59
60
61
62
63
64
65

- 1
2
3
4
5
6
7
8 [24] Y. Bazilevs, V. M. Calo, J. A. Cottrell, J. A. Evans, T. J. R. Hughes, S. Lipton, M. A.
9 Scott, T. W. Sederberg, Isogeometric analysis using T-splines, *Computer Methods in Applied
10 Mechanics and Engineering* 199 (5-8) (2010) 229–263.
- 11 [25] R. Sharma, T.-w. Kim, R. Lee Storch, H. J. Hopman, S. O. Erikstad, Challenges in computer
12 applications for ship and floating structure design and analysis, *CAD* 44 (2012) 166–185.
- 13
14 [26] H. J. Koelman, A Mid-Term Outlook on Computer Aided Ship Design, in: *COMPIT’13
15 Proceedings of the 12th International Conference on Computer Applications and Information
16 Technology in the Maritime Industries*, Ancona, Italy, 2013, pp. 110–119.
- 17
18 [27] T. W. Sederberg, J. Zheng, X. Song, Knot intervals and multi-degree splines, *Computer Aided
19 Geometric Design* 20 (2003) 455–468.
- 20
21 [28] T. W. Sederberg, D. L. Cardon, G. T. Finnigan, N. S. North, J. Zheng, T. Lyche, T-spline
22 simplification and local refinement, *ACM Transactions on Graphics* 23 (2004) 276–283.
- 23
24 [29] M. A. Scott, M. J. Borden, C. V. Verhoosel, T. W. Sederberg, T. J. R. Hughes, Isogeometric
25 finite element data structures based on Bézier extraction of T-splines, *International Journal
26 for Numerical Methods in Engineering* 88 (2) (2011) 126–156.
- 27
28 [30] M. Scott, X. Li, T. Sederberg, T. Hughes, Local refinement of analysis-suitable T-splines,
29 *Computer Methods in Applied Mechanics and Engineering* 213-216 (2012) 206 – 222.
30 doi:<http://dx.doi.org/10.1016/j.cma.2011.11.022>.
31 URL <http://www.sciencedirect.com/science/article/pii/S0045782511003689>
- 32
33 [31] M. J. Borden, M. A. Scott, J. A. Evans, T. J. R. Hughes, Isogeometric Finite Element
34 Data Structures based on Bezier Extraction of NURBS, *International Journal for Numerical
35 Methods in Engineering* 87 (2011) 15–47.
- 36
37 [32] H. Lamb, *Hydrodynamics*, 6th Edition, Cambridge Univ. Press., 1932.
- 38
39 [33] L. Milne-Thomson, *Theoretical Hydrodynamics*, 5th Edition, McMillan, 1974.
- 40
41 [34] A. I. Ginnis, R. Dunigneau, C. Politis, K. V. Kostas, K. Belibassakis, T. Gerostathis, P. D.
42 Kaklis, A multi-objective optimization environment for ship-hull design based on a bem-
43 isogeometric solver, in: *The fifth Conference on Computational Methods in Marine Engineer-
44 ing (Marine 2013)*, Hamburg, Germany, on 29-31 May 2013, 2013.
- 45
46
47
48
49
50
51
52
53
54
55
56
57
58
59
60
61
62
63
64
65